Incorporating the Effects of Tread Pattern in a Dynamic Tire Excitation Mechanism

T. G. CLAPP AND A. C. EBERHARDT

A basic understanding of dynamic tire tread response is provided and the information is incorporated in a method for predicting tire-pavement contact forces to excite dynamic tire models. Tire tread is analyzed to determine the response at the tire carcass line to external loading conditions. Results show that dynamic tread response below the natural frequency of the tread may be considered quasi-static. Static analysis shows negligible stress concentration effects at the tread edges along the carcass line. Noncontacting ribs produce vertical stress that is approximately 95 percent of the average stress along the carcass line directly below closely spaced tread elements. Tread and road surface input are combined to include the distributive effects of the tread with the higher-frequency surface effects. This is accomplished by discretizing the contact region into a finite number of equally sized elements. The pressure is computed for each element based on the tread pattern, the global pressure distribution, and the road surface input. The average pressure is determined by equating the axle loading force with the sum of the elemental pressures times elemental areas. Then the force distribution is computed over the tire-pavement contact region. Dynamic force response is determined by shifting the road and tread information and computing the force distribution for consecutive time steps.

When a loaded tire is rolled, time-varying stresses of an impulsive nature are exerted on the tire's contact surface due to rotation and the discrete nature of the tread element design. There also exists a spatial variation of the stress over the contact region due to the imposition and relaxation of loads on the tread elements while going through the footprint. A basic understanding of the excitation mechanism produced by tire-pavement interaction is an essential part of predicting the dynamic response created by tire design and construction. The dynamic nature of the forcing function is such that, as a rolling tire tries to maintain instantaneous equilibrium, fluctuating forces primarily at the leading and trailing edges of the tire produce a vibrational response that affects tire performance.

The trend by automotive manufacturers to produce small, lightweight vehicles has increased the significance of structure-borne vibration and acoustic radiation generated by a rolling tire. Road-tire-induced noise transmission paths are responsible for approximately 36 percent of the interior vehicle sound energy *(1)*. Tire noise is a major source of environmental pollution. Experimental evidence has identified tire surface vibration to be a dominant sound generation mechanism *(2)*.

North Carolina State University, Raleigh, N.C. 27695.

Tire noise, passenger comfort, and other performance criteria are affected by the dynamic response of the pneumatic tire at frequencies up to 2,000 Hz. Recent efforts to understand and predict dynamic response have led to the development of various tire models *(3–6)*. These models are attempting to predict dynamic tire response at frequencies in the audible range up to 1,000 Hz. Present dynamic models are limited in the complexity to which the tread pattern can be represented. Most tire models add tread structural properties such as stiffness and mass in the tread region, but no or very simple tread pattern information is included. The tire designer would like to model the dynamic response given a selected tread pattern. If a treadless tire model is to respond as if tread were present on the tire, the force input must reflect the tread pattern at the point where the forces enter the model and not the contact surface.

The tire excitation mechanism is dependent on many parameters such as external load, tire inflation pressure, road surface texture, and tread pattern. The tread pattern controls the transmission of tire-pavement contact forces to the tire carcass. Much work has been done to determine the global dynamic force distribution over the tire-pavement contact region *(7, 8)*. Other investigation have predicted road surface texture induced contact forces *(9, 10)*. The contact force or pressure at the tire-pavement interface must be combined with the tread pattern information to predict the excitation mechanism at the tire carcass line as required by treadless dynamic models. An important aspect in the development of an excitation mechanism is understanding how the forces are transmitted and transformed through the tread to the tire carcass.

This paper provides a basic understanding of tread response to dynamic contact forces. Dynamic analysis of a finite element tread model is performed to evaluate the carcass line response to an impulsive contact force. Stress concentrations at the carcass line are considered. The effects and influence of noncontacting ribs in the tread pattern are also investigated. The results of this paper are used to develop a tire excitation mechanism that predicts the excitation forces as they enter the tire carcass.

DYNAMIC TREAD ANALYSIS

Dynamic analysis is used to provide an understanding of the carcass line response to tread design features when loaded. Information concerning the dynamic response or transfer function of tire tread is obtained using transient finite element analysis. Nonlinear finite element analysis is required to model

the tire due to large deflections and large strains of the low-modulus rubber material. NASTRAN, NONSAP, and NIKE2D were computer codes considered. NIKE2D was selected because of the element formulation and graphical output capabilities.

NIKE2D is an implicit, static and dynamic, finite-deformation, finite element computer program for axisymmetric and plane strain problems in solid mechanics. The program has been developed at Lawrence Livermore Laboratory by J. O. Hallquist *(11)* by combining the latest algorithms available from a number of specialized finite element programs to increase the problem-solving capabilities while minimizing operating time and machine storage.

Developing a tread model for transient dynamic analysis is performed by understanding and then determining the governing parameters such as upper frequency of interest, material properties, and the number of time steps. The model is then built based on the combination of the finite element limitations and the model parameters.

Experimental evidence *(12)* shows that 16 elements per wavelength are needed to analyze transient excitation and that two time steps per element are needed to allow wave propagation without distortion. Thirty-two time steps per wavelength are therefore required. These strict limitations control the modeling parameters for the propagation of compressive waves.

The compressive wave speed is a material parameter determined by the following formula:

$$C = (Eg/r)^{1/2} \tag{1}$$

where

C = wave speed,
E = modulus of elasticity,
g = gravitational acceleration, and
r = weight density.

To illustrate Equation 1, an example using tread material properties for a typical radial passenger tire (*13*, p. 881) is presented. Other material properties may be used for particular tread compounds. The example material with properties of 520 psi (3.6 MPa) modulus and a weight density of 0.0415 lb/in.^{3} (1.15 g/cm^3) has a characteristic wave speed of 2,200 in./sec (55.9 m/sec). The shortest wavelength of interest is determined by the following formula:

$$L = C/f \tag{2}$$

where L is the wavelength and f is the upper frequency of interest.

The finite element limitation of 32 time steps per wavelength controls the time sampling increment t, which is given by

$$t = (L/C)/32 \tag{3}$$

A frequency of 2,500 Hz is selected as the upper range for proper finite element response. The resulting sampling time increment of 0.0125 msec produces a Nyquist frequency of 40 kHz. This large frequency range requires a sufficiently large number of time steps to achieve the frequency resolution necessary for analyzing frequency response in the 0- to 2,500-Hz range of interest. Computational restrictions limit the number of time steps that may be performed; consequently, 128 time steps are computed to produce a 64-line spectrum with a frequency bandwidth of 625 Hz.

With the characteristic wavelength and the number of time steps determined, the finite element tread model is constructed as shown in Figure 1. The characteristic finite element dimension of 0.060 in. (1.52 mm) is selected to obtain the limitation of 16 elements per wavelength. A symmetry boundary condition is applied along the left side of the model. The model height is determined so that a reflection of the initial wave propagation does not affect the nodal response at the carcass line.

An impulsive point force load is applied to the contact surface at the symmetry line to excite frequencies through the 2,500-Hz range as shown in Figure 2. The discrete load incre-

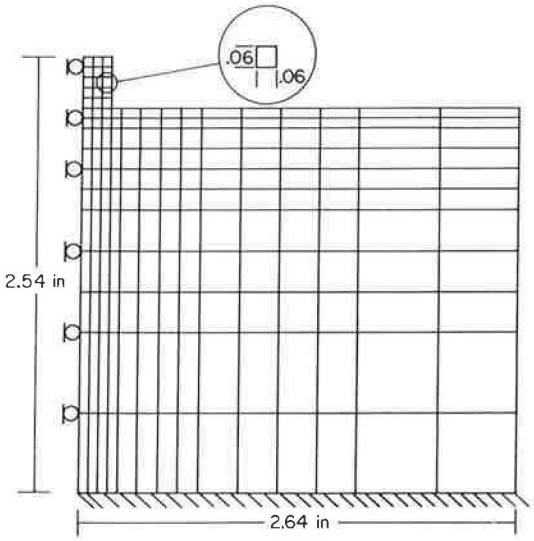

FIGURE 1 Finite element tread model for dynamic analysis.

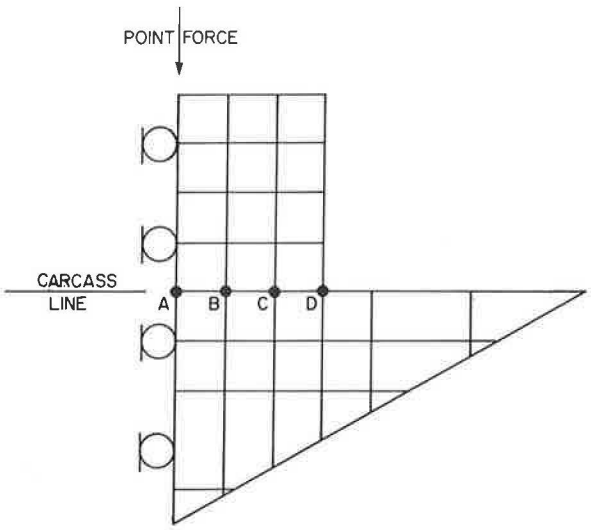

FIGURE 2 Dynamic finite element model of a tread's carcass line response to an impulsive point force.

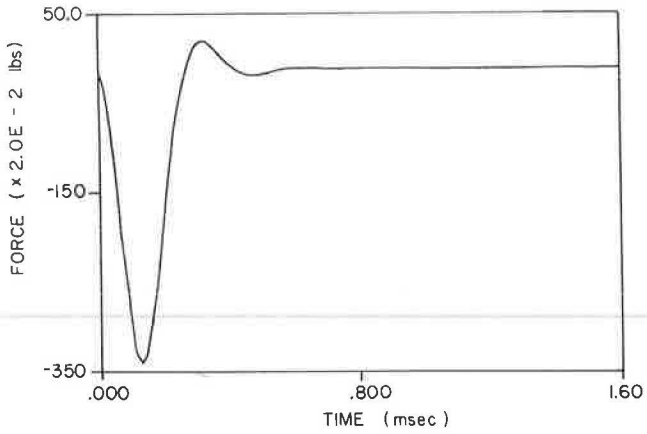

FIGURE 3 Impulsive point force input for dynamic analysis.

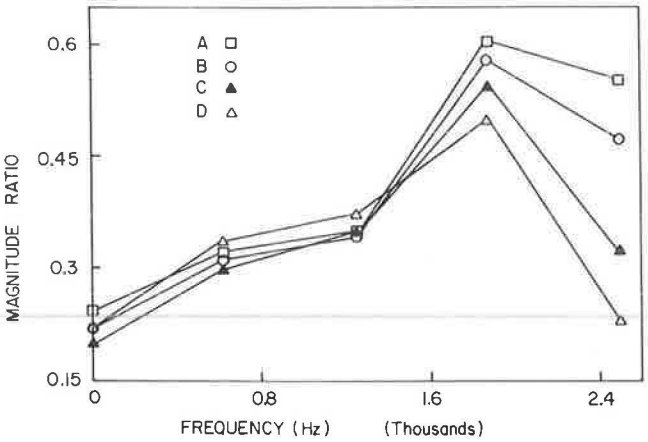

FIGURE 5 Magnitude frequency response of carcass line nodes to an impulsive point force.

ments for each time step are generated by inversely transforming a digitally filtered power spectrum in the frequency domain. The impulsive nature of the applied force input is shown in Figure 3.

The vertical stress at the driving point and at the four nodes along the carcass line is computed and stored for all 128 time steps. An example of the stress output of the driving point and a carcass line point is shown in Figure 4. The figure shows the impulsive nature of the driving point stress and the associated delayed response at the carcass line.

The four carcass line nodes located from the symmetry line to the edge of the tread are designated as *A*, *B*, *C*, and *D*, as shown in Figure 2. The magnitude and phase of the frequency response function are computed using the driving point vertical stress as input and the vertical stress at each of the carcass line nodal points as output.

The frequency response magnitude ratios are generally below 0.5 as shown in Figure 5. The phase results reflect an almost linear phase shift as shown in Figure 6. The frequency response at each nodal location is similar except for the magnitudes at 1,875 and 2,500 Hz. This fact implies that the dynamic response to a point force input is evenly distributed along the carcass line at frequencies below the 1,875-Hz bandwidth. The peak in magnitude at 1,875 Hz is of particular interest.

The simplest model of the tread element would be to treat the tread as a quarter-wavelength rod attached to an infinite medium as shown in Figure 7. Theoretically, the maximum-magnitude response occurs at the fundamental frequency of this system with lesser peaks at the higher harmonics. The theoretical natural frequency of the tread element model with a height of 0.3 in. (0.7 cm), or a 1.2-in. (3-cm) wavelength and a wave speed of 2,200 in./sec (55.9 m/sec), is 1,833 Hz, which falls within the 625-Hz bandwidth around the 1,875-Hz center frequency. Consequently, a simple rod model can provide a rough estimate of tread natural frequency and supports the dynamic finite element analysis of the tread.

This basic dynamic analysis allows a quasistatic assumption to be made as to the tread response at frequencies below the tread natural frequency. In this region, the dynamic tread response is similar to the static response. Static analysis can now be performed to understand how the contact forces are distributed below the tread at the carcass line.

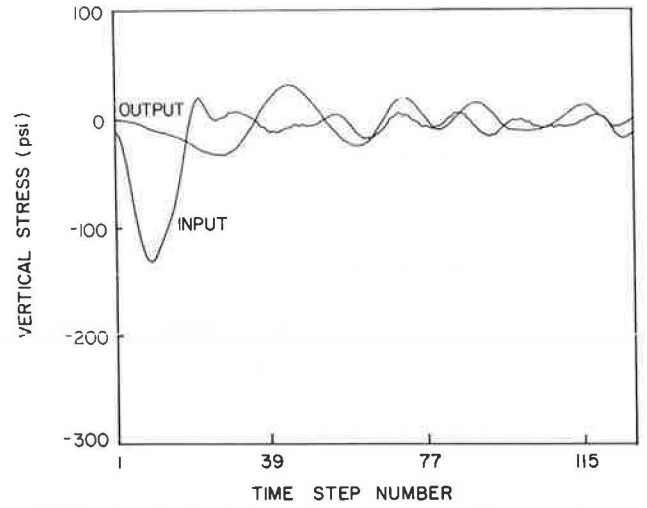

FIGURE 4 Vertical stress time response of the input driving point and an output carcass line node.

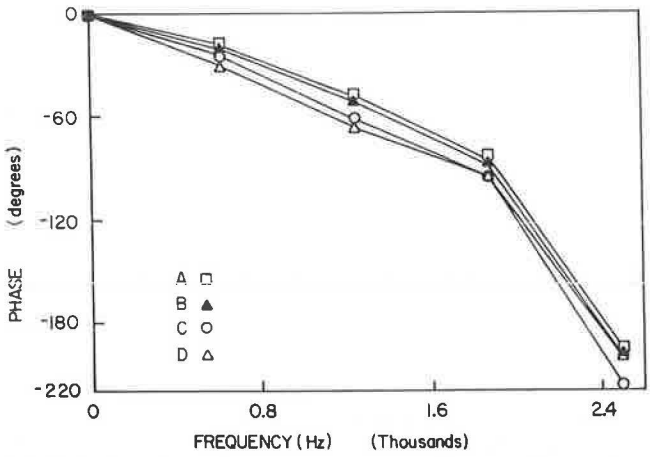

FIGURE 6 Phase frequency response of carcass line nodes to an impulsive point force.

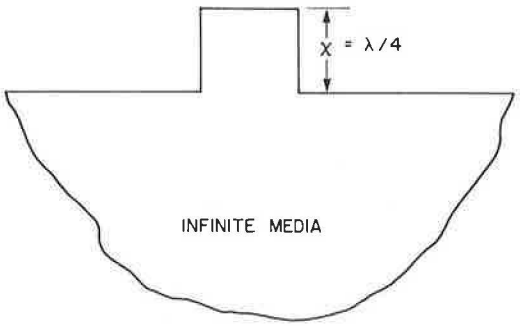

FIGURE 7 Quarter-wavelength rod model connected to an infinite medium.

STATIC TREAD RESPONSE

Various finite element tread models are analyzed statically to determine the effect of stress concentrations at the carcass line and the effect of noncontacting ribs that connect adjacent tread sections. The tread models are loaded using uniform displacement boundary conditions as shown in Figure 8. This loading condition closely simulates smooth road contact and produces a nonuniform vertical pressure distribution along the carcass line. Uniform displacement boundary conditions generate stress concentrations along the contact edges.

The significance of stress concentrations is determined by modeling the worse case, which is a tread with square edges as shown in Figure 8. The model is subjected to uniform displacement boundary conditions along the contact surface. The vertical stress produced at the carcass line is approximately 25 percent larger at the edges than at the center of the tread. Actual tread elements have a stress concentration factor much less than 1.25 because of the curved edges that must be present for the molding process; consequently, the nonuniform contact stress is distributed much more evenly across the carcass line than the contact line. This observation provides a basis for assuming that the stress concentration effect is not included in the force modeling process at the carcass line.

Tire tread design includes many considerations besides the actual contact surface involved. The assumption that the forces are transferred to the carcass line at locations only directly below the contact line excludes many sophisticated details associated with tread design. Tread designs include noncontacting ribs of various heights that connect tread elements. The noncontacting ribs produce vertical stress at the carcass that must be included in some fashion in the total tread-induced force model to ensure that these important design features are reflected in the force input.

Finite element models of differently sized and spaced ribs between two contacting tread elements are analyzed to determine the carcass line vertical stress response to uniform displacement of the contact surface. Tread spacing and rib height are the principal parameters of interest in the analysis.

The first set of finite element models has tread spacing of 0.2 in. (0.51 cm) with connecting rib height to tread height ratios of 0.25, 0.5, and 0.75. Each model is uniformly displaced at the contact surface. The vertical stress along the carcass is computed for five nodes located from the center of the rib into the tread element. The five nodes are labeled consecutively as shown in Figure 9. Nodes 2 through 5 are directly below the contact surface and Node 1 is a rib node. The vertical stress results are normalized to the minimum stress value directly below the contact surface to provide a relative scale factor at the nodal locations.

The normalized vertical stress results are graphically displayed in Figures 9–11 for rib height to tread height ratios of 0.25, 0.5, and 0.75 with a tread spacing of 0.2 in. (1.0 cm). The results show the carcass line stress carried by a noncontacting rib. The noncontacting rib with a rib height to tread height ratio of 0.25 produces carcass line stresses that exceed half the average stress under contacting tread. At rib height to tread

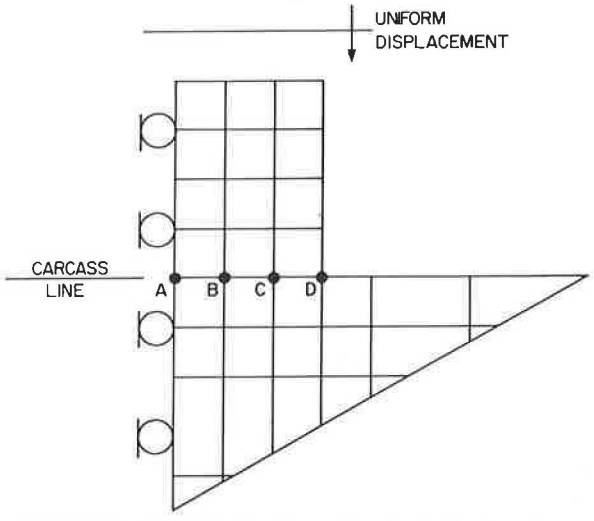

FIGURE 8 Static finite element model of a tread carcass line response to uniform displacement loading conditions.

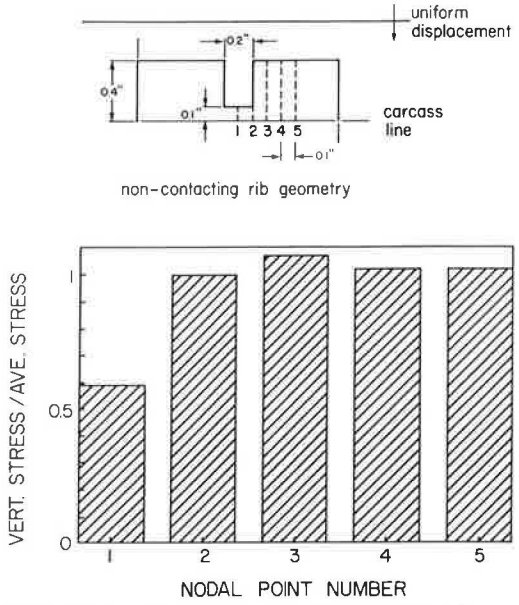

FIGURE 9 Carcass line nodal response of tread spaced 0.2 in. (0.51 cm) apart with a connecting rib of 25 percent height ratio.

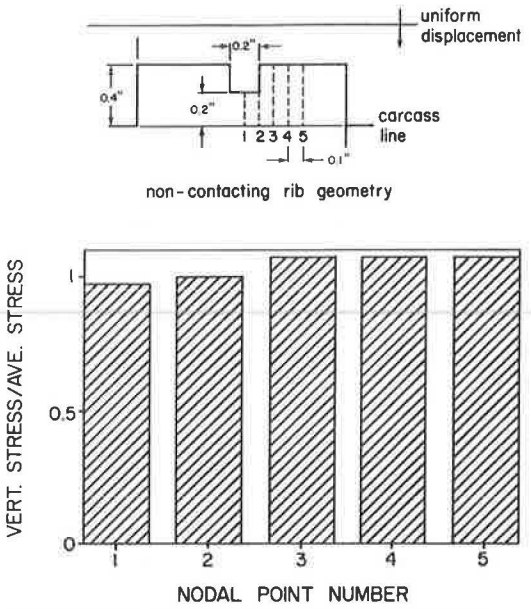

FIGURE 10 Carcass line nodal response of tread spaced 0.2 in. (0.51 cm) apart with a connecting rib of 50 percent height ratio.

height ratios of 0.50 and greater, the percentage of stress contribution to the carcass line is practically equal to the average stress over the contact region. A general statement can be made that the carcass line response of ribs with a height of greater than 50 percent of the tread height, and span between tread elements spaced less than 0.2 in. (0.51 cm) apart, is approximately equivalent to the average carcass line stress below the contact surface.

A second set of models has a tread spacing of 0.4 in. (1.0 cm) with connecting rib height to tread height ratios of 0.25, 0.50, and 0.75. Similar trends exist in distantly spaced tread elements with connecting ribs as with closely spaced tread elements except the stresses under the noncontacting ribs are lower at each rib height to tread height ratio.

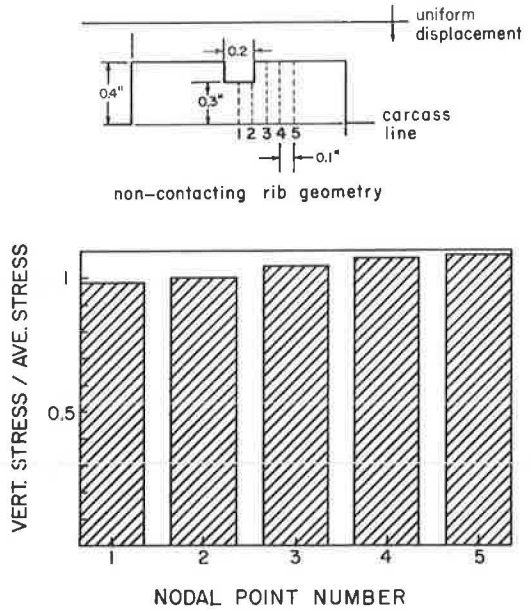

FIGURE 11 Carcass line nodal response of tread spaced 0.2 in. (0.51 cm) apart with a connecting rib of 75 percent height ratio.

The noncontacting rib results show how the vertical stress at the rib nodes increases as the height increases. The rib stress also decreases in magnitude as the tread spacing increases from the edge of the tread to the centerline of the rib. General estimates of the noncontacting rib contribution to vertical stress input at the carcass line can be made from these results.

DEVELOPMENT OF TREAD-INDUCED CONTACT FORCES

The analysis of noncontacting rib effects and tread edge effects at the carcass line provides information necessary to predict the tread-induced force input that is sensitive enough to characterize a detailed tread pattern. The way in which this information is incorporated into the tread-induced force model is by generating a tread pattern matrix. This matric has values that can range from 0 to 1, where 0 represents no tread contribution at the carcass line and 1 represents tread contact. Noncontacting ribs are represented as fractions according to rib height and tread spacing. Detailed estimates from the tread pattern values can be extracted from Figures 9–11. For passenger car tire design most of the noncontacting ribs are between contacting tread elements that are spaced less than 0.2 in. (0.51 cm) apart. When this is the case, general tread pattern scale factors for noncontacting ribs are assigned values of 0.95 and 0.6 for rib height to tread height ratios greater than 0.5 and less than 0.5, respectively.

The matrix of tread pattern values provides a scaling mechanism that can be combined with the contact region global pressure distribution. The global pressure distribution is defined as the distribution of contact pressure across the length and width of the contact patch of a rolling treadless tire. The global information is normalized to some unknown average pressure, resulting in a distribution of pressure ratios over the contact region. The unknown average pressure is determined from the equilibrium condition. Consequently, the tread-induced pressure input for an incremental area with center coordinates x and y is represented by the following formula:

$$P(x, y) = T(x, y)*G(x, y)*P_{avg} \quad (4)$$

where

$P(x, y)$ = elemental pressure,
$T(x, y)$ = tread pattern scale factor,
$G(x, y)$ = global pressure distribution, and
P_{avg} = average pressure.

In order to determine the elemental pressures, the average pressure P_{avg} must be computed. Equilibrium requires that the applied axle load must equal the sum of the incremental pressures times the incremental areas:

$$Ft = \Sigma [P(x, y)*A] \quad (5)$$

TABLE 1 SAMPLE ROAD AND TREAD DATA

Element No.	*R(x,I)* (psi)	*G(x,I)*	*T(x,I)*	IT*(x,I)*
1	0	1.2	1	1
2	20	1.3	1	1
3	30	1.4	1	1
4	15	1.5	1	1
5	0	1.5	0.95	0
6	9	1.3	0.95	0
7	0	1.2	1	1
8	7	1.2	1	1
9	15	1.2	0	0
10	4	1.1	0	0
11	0	1.1	1	1
12	0	1.0	1	1

NOTE: Ft = 75 lb; $A = 0.125$ in.^{3}.

where Ft is the static axle load and A is the element of area.

The average pressure is determined by substituting Equation 4 into Equation 5 and rearranging terms to obtain:

$$P_{avg} = (\text{Ft}/A)/\{\Sigma\,[T(x, y)*G(x, y)]\} \quad (6)$$

When no road-induced input is introduced, Equations 4 and 6 provide the basic force generation over the contact region.

When the texture-induced forces are considered, the pressure over an incremental area in the contact region is determined as

$$P(x, y) = G(x, y)*T(x, y)*P_{avg} + R(x, y)*\text{IT}(x, y) \quad (7)$$

where

$P(x, y)$ = elemental pressure,
$G(x, y)$ = global pressure distribution,
$T(x, y)$ = tread pattern data,
$R(x, y)$ = texture-induced pressure data,
IT(x, y) = integer tread pattern data, and
P_{avg} = average pressure.

Equation 7 includes the distributed contribution of the contact stress. An impulsive texture-induced pressure is included where road surface texture adds additional stress. This component is multiplied by an integer tread pattern value IT(x, y), which is either 0 or 1.

In order to determine the elemental input force, the average pressure must be determined. Equation 7 is substituted into Equation 5 and rearranged to obtain

$$P_{avg} = \{[\text{Ft}/A] - \Sigma\,[R(x, y)*\text{IT}(x, y)]\}/\{\Sigma\,[G(x, y)*T(x, y)]\} \quad (8)$$

An illustrative example is provided to explain the application of Equation 7 using a two-dimensional tread-road contact length. Necessary input data are provided in Table 1.

Recall that (a) the road-induced data $R(x, y)$ contain pressure information only at locations where the texture produces additional tire deformation, (b) the global pressure distribution $G(x, y)$ is a ratio of the global pressure at a particular location over some average pressure, (c) the tread pattern data $T(x, y)$ reflect not only the tread contact locations but also the noncontacting ribs (as seen by the two 0.95 values), and (d) the integer tread pattern IT(x, y) includes only the contacting tread locations.

For the sample data, Equation 8 is used to compute an average pressure of 41 psi (283 kPa), which is substituted into Equation 7 to produce the incremental pressure results presented in Table 2. The incremental force input is computed as the product of the pressure values times area.

This distribution of pressure values reflects the various parameter contributions, including important tread pattern information, while adding the road surface input that tends to randomize the output and to reflect the dynamic high-frequency response at the carcass line.

CONCLUSIONS

This research provides a method for developing a tire excitation mechanism that includes complex tread pattern effects. The tread effects are determined at the tire carcass to provide realistic input to treadless dynamic tire models.

Tread pattern information is generated from the tread response results by assigning a matrix of tread pattern values that range from 0 to 1 to describe the tread pattern design features over the tire-pavement contact region.

Tread and road surface texture-induced input are combined to include the distributive effects of the tread and the high-frequency road effects. This is accomplished by discretizing the contact region into a finite number of equally sized elements. The pressure is determined for each element from the tread pattern, the global pressure distribution, and the road surface input. The average pressure is determined by equating the axle loading force with the sum of the elemental pressures times element area. A discretized matrix of pressure values can be computed over the entire footprint. This would provide force data for one time stop of a dynamic tire model.

New tread and road surface information corresponding to the location of the tire contact region at the next time step can be input into the excitation model to compute the next force values required by the dynamic model. In this manner, the contact forces at the tire carcass line are predicted for a rolling tire on a desired road surface at a desired velocity.

The method developed within this report is based on many

TABLE 2 PRESSURE RESULTS FROM SAMPLE INPUT DATA

	Element No.											
	1	2	3	4	5	6	7	8	9	10	11	12
P(x, I) (psi)	49	75	93	80	58	51	49	57	0	0	45	41
P(x, I) (kPa)	305	519	644	548	403	349	339	392	0	0	311	283

simplifying assumptions. Much refinement is anticipated as knowledge is developed of true dynamic tire-pavement contact forces. This method does provide a means by which complex tread pattern information can be incorporated into sophisticated dynamic tire models.

ACKNOWLEDGMENT

The authors wish to thank Firestone Tire & Rubber Company for support of this research through the Department of Mechanical and Aerospace Engineering at North Carolina State University.

REFERENCES

1. S. K. Jha. Identification of Road/Tyre Induced Noise Transmission Paths in a Vehicle. *International Journal of Vehicle Design and Components*, Vol. 5, Nos. 1–2, Jan. 1984, pp. 143–158.
2. A. C. Eberhardt. *An Experimental and Analytical Investigation of the Vibration Noise Generation Mechanism in Truck Tires*. Report DOT-HS-8-02020. U.S. Department of Transportation, March 1981.
3. D. E. Southworth. *Finite Element Modeling and Verification of Heavy Vehicle Tire Transient Response*. Master's thesis. North Carolina State University, Raleigh, 1984.
4. M. C. Goff. *Development of a 3-Dimensional Finite Element Model of Orthotropic Laminate Tire Structures Under Initial Pressure Loading for Model Response*. Master's thesis. North Carolina State University, Raleigh, 1985.
5. F. Tabaddor and J. R. Stafford. Nonlinear Vibration of Cord-Reinforced Composite Shells. *Computers and Structures*, Vol. 13, 1981, pp. 737–743.
6. Y. B. Chang, T. Y. Yang, and W. Soedel. Dynamic Analysis of a Radial Tire by Finite Element and Model Expansion. *Journal of Sound and Vibration*, Vol. 96, No. 1, 1981, pp. 1–11.
7. S. A. Lippmann and K. L. Oblizajek. The Distributions of Stress Between the Tread and the Road for Freely Rolling Tires. *SAE Transactions*, 740072, 1974.
8. A. Browne, K. C. Ludema, and S. K. Clark. Contact Between the Tire and Roadway. *Mechanics of Pneumatic Tires*. NHTSA, U.S. Department of Transportation, 1981.
9. T. G. Clapp. *Approximation and Analysis of Tire/Pavement Contact Information Resulting from Road Surface Roughness*. Ph.D. dissertation. North Carolina State University, Raleigh, 1985.
10. T. G. Clapp and A. C. Eberhardt. Computation and Analysis of Texture-Induced Contact Information in Tire/Pavement Interaction. In *Transportation Research Record 1084*, TRB, National Research Council, Washington, D.C., 1986, pp. 23–29.
11. J. O. Hallquist. *NIKE2D—A Vectorized, Implicit, Finite Deformation, Finite Element Code for Analyzing the Static and Dynamic Response of 2-D Solids*. Report UCID-19677. Lawrence Livermore Laboratory, University of California, Berkeley, 1983.
12. A. C. Eberhardt. *Interaction of the Tire/Pavement Interaction Mechanism—Phase I and II*. Final Report, DOT/OST/P-34/86/036. U.S. Department of Transportation, June 1985.
13. J. R. Beatty. Physical Properties of Rubber Compounds. *Mechanics of Pneumatic Tires* (S. K. Clark, ed.), NHTSA, U.S. Department of Transportation, Washington, D.C., 1981.

Publication of this paper sponsored by Committee on Surface Properties-Vehicle Interaction.